Wide-azimuth angle-domain imaging for anisotropic reverse-time migration

Paul Sava, Center for Wave Phenomena, Colorado School of Mines
Tariq Alkhalifah, King Abdullah University of Science and Technology

SUMMARY

Extended common-image-point gathers (CIP) constructed by wide-azimuth TI wave-equation migration contain all the necessary information for angle decomposition as a function of the reflection and azimuth angles at selected locations in the subsurface. The reflection and azimuth angles are derived from the extended images using analytic relations between the space-lag and time-lag extensions. This post-imaging decomposition requires only information which is already available at the time of migration, i.e. the model parameters and the tilt angles of the TI medium. The transformation amounts to a linear Radon transform applied to the CIPs obtained after the application of the extended imaging condition. If information about the reflector dip is available at the CIP locations, then only two components of the space-lag vectors are required, thus reducing computational cost and increasing the affordability of the method. This efficient angle decomposition method is suitable for wide-azimuth imaging in anisotropic media with arbitrary orientation of the symmetry plane.

INTRODUCTION

Wave-equation depth migration is a powerful tool for accurately imaging the complex regions of the earth's interior. The quality of the image depends on the accuracy of the (anisotropic) earth model and on the technique used for wavefield reconstruction (Gray et al., 2001). This challenge can be addressed by imaging using wide-azimuth reverse-time migration (Regone, 2006; Michell et al., 2006; Clarke et al., 2006). In addition to structural imaging, it is desirable to describe reflectivity as a function of reflection angles which indicate the subsurface illumination, and could be used for model estimation and amplitude variation with angle analysis.

Angle gathers can be produced by ray methods (Xu et al., 1998; Brandsberg-Dahl et al., 2003; Koren et al., 2008) or by wavefield methods (de Bruin et al., 1990; Xie and Wu, 2002; Sava and Fomel, 2003; Biondi and Symes, 2004; Wu and Chen, 2006; Sava and Fomel, 2005; Xu et al., 2010; Sava and Vlad, 2011). In the wavefield domain, angle gathers can be constructed either before or after the application of an imaging condition. The methods operating before the imaging condition decompose the extrapolated wavefields directly (de Bruin et al., 1990; Wu and Chen, 2006; Zhu and Wu, 2010; Biondi and Tisserant, 2004; Xu et al., 2010). This type of decomposition is costly since it operates on large wavefields characterized by complex multipathing, which makes event identification challenging. The methods operating after the imaging condition decompose the images themselves which are represented as a function of space and additional parameters, typically referred to as extensions (Rickett and Sava, 2002; Sava and Fomel, 2006; Sava and Vasconcelos, 2011).

Conventionally, angle-domain imaging uses common-image-gathers (CIGs) representing the reflectivity as a function of angles and a space axis, typically the depth axis. An alternative procedure uses common-image-point-gathers (CIP) selected at various image positions. We focus on angle decomposition using extended CIPs, which offer large computational savings over alternative methods based on CIGs (Sava and Vasconcelos, 2011).

The thin layering in the Earth subsurface induces wave propagation characteristics best described by anisotropic media. Since the layering has a general preferred direction, the transversely isotropic (TI) assumption is the most appropriate to represent big parts of the subsurface. Anisotropy defines a medium in which the wave speed varies with the propagation angle. Angle gathers have a prominent role in defining such angular variations, and thus in estimating anisotropy parameters.

We develop a technique for angle-domain reverse-time migration in general TI media with arbitrary symmetry axis direction. Our technique utilizes local plane wave decompositions of extended image and exploits information about the anisotropy characterizing the imaged medium. This formulation produces an accurate description of the specular reflection for general 3D TI media, while being affordable for large-scale wide-azimuth imaging projects.

WIDE-AZIMUTH ANGLE GATHERS

Conventional seismic imaging is based on the concept of single scattering and is a process involving two steps: the wavefield reconstruction and the imaging condition. The key elements in this imaging procedure are the source and receiver wavefields, W_s and W_r which are 4-dimensional objects as a function of space $\mathbf{x} = \{x, y, z\}$ and time t. For imaging, we need to analyze if the wavefields match kinematically in time and then extract the reflectivity information using an imaging condition operating along the space and time axes (Berkhout, 1982; Clærbout, 1985)..

Wavefield reconstruction in TTI media requires a numeric solution to a pseudo-acoustic wave-equation. We use to use the time-domain method of Fletcher et al. (2009) and Fowler et al. (2010) which consists of solving

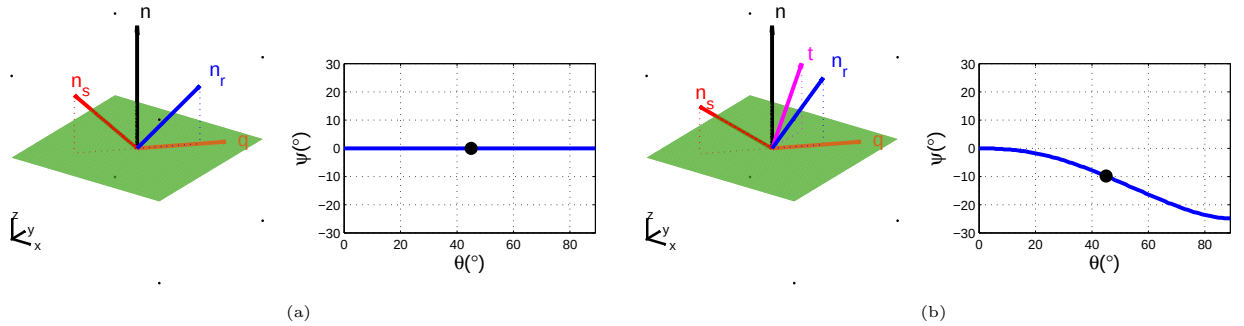

Figure 1: Reflection geometry and dependence of angle ψ with angle θ for (a) isotropic, (b) TTI materials. The large black dot in the right panels corresponds to the geometry of the vectors shown in the left panels.

a system of second-order coupled equations:

$$\frac{\partial^2 p}{\partial t^2} = v_{p_x}^2 H_2 [p] + v_{p_z}^2 H_1 [q] \ , \quad (1)$$

$$\frac{\partial^2 q}{\partial t^2} = v_{p_n}^2 H_2 [q] + v_{p_z}^2 H_1 [q] \ . \quad (2)$$

The wavefields p and q depend on space $\mathbf{x} = \{x, y, z\}$ and time t. H_1 and H_2 are differential operators applied to the wavefields in the square brackets and v_{p_z}, v_{p_x}, and v_{p_n} are the vertical, horizontal and "NMO" velocities used to parametrize a generic TTI medium: $v_{p_n} = v_{p_z}\sqrt{1+2\delta}$ and $v_{p_x} = v_{p_z}\sqrt{1+2\epsilon}$ (Thomsen, 2001). Thus, the quantities H_1 and H_2 are defined using angles θ_a and ϕ_a which describe the tilt and azimuth of the symmetry plane.

A conventional cross-correlation imaging condition based on the reconstructed wavefields can be formulated as the zero lag of the cross-correlation between the source and receiver wavefields (Clærbout, 1985):

$$R(\mathbf{x}) = \sum_{shots} \sum_{t} W_s(\mathbf{x}, t) W_r(\mathbf{x}, t) \, ; \, , \quad (3)$$

where R represents the migrated image which depends on position $\mathbf{x}$. An extended imaging condition preserves in the output image certain acquisition (e.g. source or receiver coordinates) or illumination (e.g. reflection angle) parameters (Rickett and Sava, 2002; Sava and Fomel, 2005, 2006; Sava and Vasconcelos, 2011):

$$R(\mathbf{x}, \boldsymbol{\lambda}, \tau) = \sum_{shots} \sum_{t} W_s(\mathbf{x} - \boldsymbol{\lambda}, t - \tau) W_r(\mathbf{x} + \boldsymbol{\lambda}, t + \tau) \ . \quad (4)$$

These extensions can be converted to reflection angles (Sava and Fomel, 2003, 2006; Sava and Vlad, 2011), thus enabling analysis of amplitude variation with angle for images constructed in complex areas using wavefield-based imaging. The problem we are solving here is to decompose extended CIPs as a function of azimuth ϕ and reflection θ angles at selected points in the image: $R(\boldsymbol{\lambda}, \tau) \Longrightarrow R(\phi, \theta, \tau)$. However, we assume that all parmeters characterizing the anisotropic medium are known. Therefore, all the energy in the output CIPs concentrates at $\tau = 0$, so we can focus our attention on a particular case of the decomposition which does not preserve the time-lag variable in the output.

An implicit assumption made by all methods of angle decomposition is that we can describe the reflection process by locally planar objects. Such methods assume that (locally) the reflector is a plane, and that the incident and reflected wavefields are also (locally) planar. Only with these assumptions we can define vectors in-between which we measure angles like the angles of incidence and reflection, as well as the azimuth angle of the reflection plane.

Our method uses this assumption explicitly, although we do not assume that the wavefronts of the source and receiver wavefields are planar. We consider each wavefront as a superposition of planes with different orientations and treat each one of these planes separately in the angle decomposition. Then, we can write the conventional imaging condition as

$$\hat{\mathbf{n}}_s \cdot (\mathbf{x} - \mathbf{x}_s) = v_s (t - t_p) \ , \quad (5)$$

$$\hat{\mathbf{n}}_r \cdot (\mathbf{x} - \mathbf{x}_r) = v_r (t - t_s) \ . \quad (6)$$

This system indicates that the source and receiver wavefields are coincident in space at a given time. Here $v_s(\theta, \phi)$ and $v_r(\theta, \phi)$ are velocities for the source and receiver wavefields which depend on the reflection angles θ and ϕ. For the case of PP reflections in isotropic media, or in DTI media Alkhalifah and Sava (2010) we have that $v_s = v_r$. Similarly, we can write the extended imaging condition as

$$\hat{\mathbf{n}}_s \cdot (\mathbf{x} - \mathbf{x}_s - \boldsymbol{\lambda}) = v_s (t - t_p - \tau) \ , \quad (7)$$

$$\hat{\mathbf{n}}_r \cdot (\mathbf{x} - \mathbf{x}_r + \boldsymbol{\lambda}) = v_r (t - t_s + \tau) \ , \quad (8)$$

where $\boldsymbol{\lambda}$ and τ are lags in space and time. The delay is relative to the position and time identified by the conventional imaging condition, equations 5-6. Substituting equation 5 in 7 and equation 6 in equation 8, we obtain the expressions

$$\hat{\mathbf{n}}_s \cdot \boldsymbol{\lambda} = v_s \tau \ , \quad (9)$$

$$\hat{\mathbf{n}}_r \cdot \boldsymbol{\lambda} = v_r \tau \ . \quad (10)$$

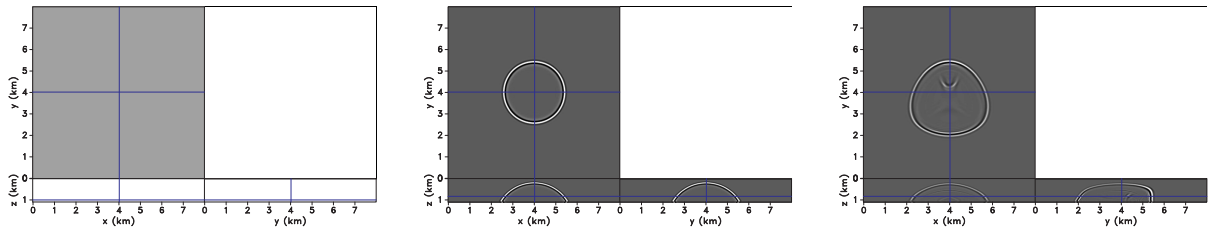

(a) (b) (c)

Figure 2: (a) Velocity model for the synthetic experiments. The horizontal reflector is located at $z = 1$ km and the sources are distributed on the surface on a regular grid with separation of 0.4 km in x and y. Wavefield snapshots for (b) isotropic, and (c) TTI materials.

Expressing the normal vectors $\hat{\mathbf{n}}_s$ and $\hat{\mathbf{n}}_r$ as a function of the normal vector $\hat{\mathbf{n}}$ and the vector $\hat{\mathbf{q}}$ at the intersection of the reflection and the reflector plane, we obtain

$$(\hat{\mathbf{q}} \cdot \boldsymbol{\lambda}) \sin\theta_s - (\hat{\mathbf{n}} \cdot \boldsymbol{\lambda}) \cos\theta_s = v_s \tau \,, \quad (11)$$

$$(\hat{\mathbf{q}} \cdot \boldsymbol{\lambda}) \sin\theta_r + (\hat{\mathbf{n}} \cdot \boldsymbol{\lambda}) \cos\theta_r = v_r \tau \,, \quad (12)$$

where θ_s and θ_r are the (phase) angles made by the source and receiver wavefronts with the normal.

We can separate the quantity $(\hat{\mathbf{q}} \cdot \boldsymbol{\lambda})$ from equations 11 and 12 and the quantity $(\hat{\mathbf{n}} \cdot \boldsymbol{\lambda})$ from equations 11 and 12 and using Snell's law $v_r \sin\theta_s - v_s \sin\theta_r = 0$ we obtain

$$(\hat{\mathbf{q}} \cdot \boldsymbol{\lambda}) \sin(\theta_s + \theta_r) = [v_s \cos\theta_r + v_r \cos\theta_s]\, \tau \,, \quad (13)$$

$$(\hat{\mathbf{n}} \cdot \boldsymbol{\lambda}) \sin(\theta_s + \theta_r) = 0 \,. \quad (14)$$

The calculations simplify and become more symmetric if we make the notations $2\theta = \theta_r + \theta_s$ and $2\psi = \theta_r - \theta_s$. The angle 2θ represents the sum of the reflection angles on the source and receiver sides, and the angle 2ψ represents their difference. If we label γ the ratio of the velocities on the source and receiver sides, we have

$$\tan\psi = \frac{1-\gamma}{1+\gamma} \tan\theta \,. \quad (15)$$

For isotropic, VTI or DTI media, we have that $\gamma = 1$, therefore $\tan\psi = 0$ regardless of the angles of incidence or reflection, θ_s and θ_r. Otherwise, the angle ψ depends on the opening angle θ and on the material properties at the reflection point, i.e. the velocities v_s and v_r. On the other hand, the velocities v_s and v_r depend on the angles θ and ψ, thus leading to a circular dependency.

With this notation, we can write the system 13-14 as

$$(\hat{\mathbf{q}} \cdot \boldsymbol{\lambda}) \sin(2\theta) = [v_s \cos(\theta + \psi) + v_r \cos(\theta - \psi)]\, \tau \,, \quad (16)$$

$$(\hat{\mathbf{n}} \cdot \boldsymbol{\lambda}) = 0 \,. \quad (17)$$

For PP reflections in isotropic or DTI media, the system reduces to the relations derived by Sava and Vlad (2011). This system allows us to perform wide-azimuth angle decomposition applicable to anisotropic media with arbitrary tilt relative to the reflector. We describe the anisotropic medium by the vertical velocity v_{p_z}, by the anisotropic parameters ϵ and δ (Thomsen, 2001), and by the tilt vector $\hat{\mathbf{t}}$ which can take an arbitrary orientation relative to the normal vector $\hat{\mathbf{n}}$.

At every CIP location, we use the information about the known normal vector $\hat{\mathbf{n}}$, measured from the image, and the azimuth reference vector $\hat{\mathbf{v}}$ to compute a reference in the reflection plane, $\hat{\mathbf{a}}$. Then, we loop over all possible values of the azimuth angle ϕ to compute. Here we first need to evaluate the angle ψ defined in the preceding section. This calculation cannot be done analytically due to the circular dependence between the velocities and phase angles in anisotropic media, but requires a numeric solution. One possibility is to loop over all possible values of the angle ψ and select the one for which Snell's law is best satisfied. The algorithm consists of the following steps: (1) Evaluate the incidence and reflection angles, θ_s and θ_r; (2) Evaluate the incidence and reflection vectors, $\hat{\mathbf{n}}_s$ and $\hat{\mathbf{n}}_r$, by a simple rotation of the normal vector $\hat{\mathbf{n}}$ with angles θ_s and θ_r; (3) Evaluate the angles α_s and α_r between the incidence and reflection vectors and the tilt vector, $\hat{\mathbf{t}}$; (4) Evaluate the velocities corresponding to angles α_s and α_r relative to the tilt vector (Tsvankin, 2005); (5) Evaluate a function characterizing Snell's law $S(\psi) = v_r \sin\theta_s - v_s \sin\theta_r$ and decide if the chosen value of ψ minimizes the function $S(\psi)$. Finally, we apply a slant-stack to the CIP cube $R(\boldsymbol{\lambda}, \tau)$ using equations 16 and 17 using the velocities computed before. We obtain a measure of the reflectivity as a function of the reflection angles θ and ϕ.

ANISOTROPIC ANGLE DECOMPOSITION ALGORITHM

$c = 1 \ldots N\{$
  read $\hat{\mathbf{n}}$, v_{p_z}, $\hat{\mathbf{t}}$, ϵ, δ
  $\{\hat{\mathbf{n}}, \hat{\mathbf{v}}\} \rightarrow \hat{\mathbf{a}}$
  loop $\phi = 0° \ldots 360°\{$
    $\{\hat{\mathbf{n}}, \hat{\mathbf{a}}, \phi\} \rightarrow \hat{\mathbf{q}}$
    $\theta = 0° \ldots 90°\{$
      $\{\hat{\mathbf{n}}, \hat{\mathbf{q}}, \hat{\mathbf{t}}, \theta, v_{p_z}, v_{sz}, \epsilon, \delta\} \rightarrow \{\psi, v_s, v_r\}$
      $R(\boldsymbol{\lambda}, \tau) \xrightarrow{\hat{\mathbf{q}}, \theta, \psi, v_s, v_r} R(\phi, \theta)$
    $\}$
  $\}$
$\}$

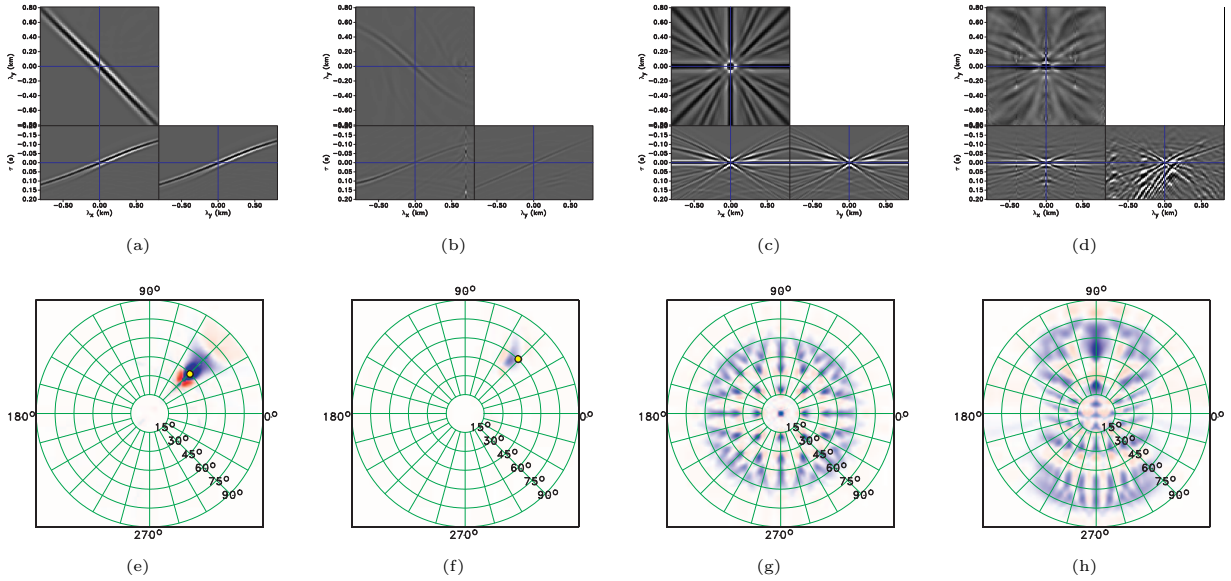

Figure 3: Extended CIPs and wide-azimuth angle gathers: (a)-(b)-(e)-(f) single-shot and (c)-(d)-(g)-(h) multi-shot imaging; (a)-(c)-(e)-(g) isotropic, and (b)-(d)-(f)-(h) TTI materials.

Figures 1(a)-1(b) illustrate the procedure described earlier. The left panels depict the vectors characterizing a particular reflection process, i.e. at a given aperture angle 2θ and azimuth $\phi = 45^\circ$, and the right panels depict the dependence of the angle ψ with the reflection angle θ. Figure 1(a) corresponds to reflections in an isotropic material, i.e. $\psi = 0$ for all θ, and 1(b) corresponds to reflections in an anisotropic medium characterized by $v_{p_z} = 3.0$ km/s, $\epsilon = 0.45$ and $\delta = -0.29$ and tilt oriented at $\theta_a = 35^\circ$ from the normal and $\phi_a = 90^\circ$ from the x axis. The angle ψ is not constant and depends on the material properties, as well as the orientation of the tilt vector and the reflection azimuth. For the special case of DTI materials, i.e. when the normal and anisotropy tilt vectors are aligned, the angle $\psi = 0$.

EXAMPLES

We illustrate our angle decomposition methodology using a simple example. The models are homogeneous, with a horizontal reflector, Figure 2(a). We consider isotropic and TTI models as described in the preceding section. Figures 2(b)-2(c) show wavefield snapshots. In the isotropic case, the moveout is azimuthally symmetric, while for the TTI case it is not.

Figures 3(a)-3(b) show the extended images obtained by reverse-time migration for one shot located on the surface at coordinates $\{x = 4, y = 4, z = 0\}$ km. The CIP analyzed here is located at $\{x = 4.7, y = 4.7, z = 1\}$ km. Figures 3(e)-3(f) show the corresponding wide-azimuth angle gathers for the extended images in Figures 3(a)-3(b), respectively. We use this geometry because the expected angles of incidence in homogeneous isotropic media are $\phi = 45^\circ$ and $\theta = 45^\circ$. The yellow dot overlain on the angle-gathers shown in Figures 3(e)-3(f) corresponds to a numeric estimation of the reflection angles using two-point ray tracing in the given TTI medium which confirms the accuracy of our angle decomposition.

Our technique can also be applied to CIPs created from many different shots. Figures 3(c)-3(h) are similar to Figures 3(a)-3(f), except that imaging is performed using shots located on a regular grid at $z = 0$ km with spacing of 0.4 km in x and y. Each shots illuminates this point in the subsurface at different angles θ and ϕ, as illustrated in Figures 3(g)-3(h). When imaging in the TTI medium, the reflection illuminate predominantly in the direction of the tilt.

CONCLUSIONS

Wide-azimuth angle decomposition can be performed on individual common-image-point gathers constructed using the extended imaging condition in space and time. The extended imaging condition is applicable equally well when migration is done with downward continuation or time reversal. The angle decomposition can separate the precise reflection angles (opening and azimuth), regardless of the complexity of wave propagation in the overburden and the heterogeneity of the model parameters. In particular, our technique does not require the TI anisotropic model to align with the reflector orientation, thus giving us full flexibility to handle arbitrary TI media. The extended common-image-point gathers encode information from all wavefield branches. Thus angle decomposition unravels all illumination directions equally well and at no additional computational cost.

REFERENCES

Alkhalifah, T., and P. Sava, 2010, A transversely isotropic medium with a tilted symmetry axis normal to the reflector: Geophysics (Letters), **75**, A19–A24.

Berkhout, A. J., 1982, Imaging of acoustic energy by wave field extrapolation: Elsevier.

Biondi, B., and W. Symes, 2004, Angle-domain common-image gathers for migration velocity analysis by wavefield-continuation imaging: Geophysics, **69**, 1283–1298.

Biondi, B., and T. Tisserant, 2004, 3D angle-domain common-image gathers for migration velocity analysis: Geophys. Prosp., **52**, 575–591.

Brandsberg-Dahl, S., M. V. de Hoop, and B. Ursin, 2003, Focusing in dip and AvA compensation on scattering-angle/azimuth common image gathers: Geophysics, **68**, 232–254.

Clærbout, J. F., 1985, Imaging the Earth's interior: Blackwell Scientific Publications.

Clarke, R., G. Xia, N. Kabir, L. Sirgue, and S. Michell, 2006, Case study: A large 3D wide azimuth ocean bottom node survey in deepwater gom: SEG Technical Program Expanded Abstracts, **25**, 1128–1132.

de Bruin, C. G. M., C. P. A. Wapenaar, and A. J. Berkhout, 1990, Angle-dependent reflectivity by means of prestack migration: Geophysics, **55**, 1223–1234.

Fletcher, R. P., X. Du, and P. J. Fowler, 2009, Reverse time migration in tilted transversely isotropic (TTI) media: Geophysics, **74**, WCA179–WCA187.

Fowler, P. J., X. Du, and R. P. Fletcher, 2010, Coupled equations for reverse time migration in transversely isotropic media: Geophysics, **75**, S11–S22.

Gray, S. H., J. Etgen, J. Dellinger, and D. Whitmore, 2001, Seismic migration problems and solutions: Geophysics, **66**, 1622–1640.

Koren, Z., I. Ravve, E. Ragoza, A. Bartana, P. Geophysical, and D. Kosloff, 2008, Full-azimuth angle domain imaging: SEG Technical Program Expanded Abstracts, **27**, 2221–2225.

Michell, S., E. Shoshitaishvili, D. Chergotis, J. Sharp, and J. Etgen, 2006, Wide azimuth streamer imaging of mad dog; have we solved the subsalt imaging problem?: SEG Technical Program Expanded Abstracts, **25**, 2905–2909.

Regone, C., 2006, Using 3D finite-difference modeling to design wide azimuth surveys for improved subsalt imaging: SEG Technical Program Expanded Abstracts, **25**, 2896–2900.

Rickett, J., and P. Sava, 2002, Offset and angle-domain common image-point gathers for shot-profile migration: Geophysics, **67**, 883–889.

Sava, P., and S. Fomel, 2003, Angle-domain common image gathers by wavefield continuation methods: Geophysics, **68**, 1065–1074.

———, 2005, Coordinate-independent angle-gathers for wave equation migration: 75th Annual International Meeting, SEG, Expanded Abstracts, 2052–2055.

———, 2006, Time-shift imaging condition in seismic migration: Geophysics, **71**, S209–S217.

Sava, P., and I. Vasconcelos, 2011, Extended imaging condition for wave-equation migration: Geophysical Prospecting, **59**, 35–55.

Sava, P., and I. Vlad, 2011, Wide-azimuth angle gathers for wave-equation migration: Geophysics, in press.

Thomsen, L., 2001, Seismic anisotropy: Geophysics, **66**, 40–41.

Tsvankin, I., 2005, Seismic signatures and analysis of reflection data in anisotropic media: Elsevier.

Wu, R.-S., and L. Chen, 2006, Directional illumination analysis using beamlet decomposition and propagation: Geophysics, **71**, S147–S159.

Xie, X., and R. Wu, 2002, Extracting angle domain information from migrated wavefield: 72nd Ann. Internat. Mtg, Soc. of Expl. Geophys., 1360–1363.

Xu, S., H. Chauris, G. Lambare, and M. S. Noble, 1998, Common angle image gather: A new strategy for imaging complex media: 68th Ann. Internat. Mtg, Soc. of Expl. Geophys., 1538–1541.

Xu, S., Y. Zhang, and B. Tang, 2010, 3D common image gathers from reverse time migration: SEG Technical Program Expanded Abstracts, **29**, 3257–3262.

Zhu, X., and R.-S. Wu, 2010, Imaging diffraction points using the local image matrices generated in prestack migration: Geophysics, **75**, S1–S9.